11-4-2011

Density Functional Theory Study on the Electronic Structure of *n*- and *p*-Type Doped $SrTiO_3$ at Anodic Solid Oxide Fuel Cell Conditions

Suwit Suthirakun
University of South Carolina - Columbia

Salai Cheettu Ammal
University of South Carolina - Columbia

Guoliang Xiao
University of South Carolina - Columbia

Fanglin Chen
University of South Carolina - Columbia, chenfa@cec.sc.edu

Andreas Heyden
University of South Carolina - Columbia, heyden@cec.sc.edu

See next page for additional authors

Publication Info

Published in *Physical Review B*, Volume 84, 2011, pages 205102-.

Density functional theory study on the electronic structure of *n*- and *p*-type doped $SrTiO_3$ at anodic solid oxide fuel cell conditions

Suwit Suthirakun,[1] Salai Cheettu Ammal,[1] Guoliang Xiao,[2] Fanglin Chen,[2] Hans-Conrad zur Loye,[3] and Andreas Heyden[1,*]

[1]*Department of Chemical Engineering, University of South Carolina, 301 South Main Street, Columbia, South Carolina 29208, USA*

[2]*Department of Mechanical Engineering, University of South Carolina, 300 South Main Street, Columbia, South Carolina 29208, USA*

[3]*Department of Chemistry and Biochemistry, University of South Carolina, 631 Sumter Street, Columbia, South Carolina 29208, USA*

(Received 3 August 2011; published 4 November 2011)

The electronic conductivity and thermodynamic stability of mixed *n*-type and *p*-type doped $SrTiO_3$ have been investigated at anodic solid oxide fuel cell (SOFC) conditions using density functional theory (DFT) calculations. In particular, constrained *ab initio* thermodynamic calculations have been performed to evaluate the phase stability and reducibility of various Nb- and Ga-doped $SrTiO_3$ at synthesized and anodic SOFC conditions. The density of states (DOS) of these materials was analyzed to study the effects of *n*- and *p*-doping on the electronic conductivity. In agreement with experimental observations, we find that the transformation from 20% Nb-doped Sr-deficient $SrTiO_3$ to a non-Sr-deficient phase occurs at high temperature and low oxygen partial pressure, which leads to a significant improvement in electronic conductivity. A mixed ionic/electronic conductor is obtained when doping 20% Nb-doped $SrTiO_3$ with small amounts of Ga (10%) in a reducing environment and high temperature. Doping with higher concentrations of Ga, e.g., 20%, diminishes the electronic conductivity of the material. These findings suggest that independent of the specific dopant, mixed ionic/electronic conductivity can be obtained in perovskite oxides under reducing conditions and high temperatures by doping the B-site with small amounts of both *n*-type and *p*-type dopants.

DOI: 10.1103/PhysRevB.84.205102 PACS number(s): 71.20.Ps, 72.80.Jc

I. INTRODUCTION

Although Ni-supported yttria-stabilized zirconia (Ni/YSZ) cermet exhibits very good catalytic activity for fuel oxidation in solid oxide fuel cells (SOFCs), it is easily poisoned by small amounts of sulfur impurities in the fuel gas.[1] Moreover, it is prone to sintering[2–4] and coking when exposed to hydrocarbon fuels.[5] As a result, exploring alternative SOFC anode materials to replace Ni/YSZ has become a crucial subject for the development of SOFC technology. Of the novel anode catalysts, perovskite-based materials have been shown to satisfy most intrinsic SOFC anode requirements such as high mixed ionic/electronic conductivity, good catalytic activity, and high thermodynamic stability at anodic conditions.[6–12] Furthermore, perovskite-based materials possess high resistance to sulfur impurities[13–15] and coke formation[5,6,16,17] since both sulfur and carbon species can easily be oxidized at the surface of the perovskite oxide.[18]

Among the numerous perovskite systems that have been explored, $SrTiO_3$-based perovskites have been widely used as alternative SOFC anode materials.[8,9,14,19] Indeed, several research groups have reported that $SrTiO_3$-based perovskites exhibit some advantages over Ni/YSZ anode catalysts, such as promising mixed ionic/electronic conductivity, adequate thermodynamic stability in a wide range of oxygen partial pressure, and tolerance to sulfur impurities as well as coke formation.[9,13–15] Moreover, it has been found that yttrium-doped $SrTiO_3$ (SYT) possesses a thermal expansion coefficient compatible with that of YSZ and Lanthanum Strontium Gallium Magnesium Oxide (LSGM)-based electrolytes.[9]

However, stoichiometric $SrTiO_3$ is a band insulator with a band gap of 3.2 eV.[20] Therefore, various dopants have been introduced to improve the electronic conductivity of this material. It is well known that doping the material with either *n*- or *p*-type dopants can enhance the degree of electronic conduction.[21–25] For example, the transformation from an insulating state to a metallic state has been observed when doping $SrTiO_3$ with *n*-type impurities such as La, Y, and Nb.[14,26–28] In addition theoretical studies have suggested that substituting Ti with *n*-type dopants can shift the Fermi level into the conduction band making the system metallic.[23,29]

It is well known that the substitution of *n*-type dopants in the $SrTiO_3$ lattice generates a defect with an effective positive charge in the host lattice. Overall electroneutrality of the lattice can be achieved by two different mechanisms, namely, electronic compensation and cation-vacancy compensation.[30–32] At low oxygen chemical potential, the formal charges of *n*-type dopants are electronically compensated by creating conduction electrons that travel along the Ti–O–Ti bridge where Ti remains mixed-valent Ti^{3+}/Ti^{4+}.[33] This electron-transferring process is considered to be the origin of the electronic conductivity of the material.[34] On the other hand at higher oxygen chemical potential the excess positive charge can be compensated by generating Sr^{2+} cation vacancies.[35] This type of electron compensation provides no conduction electrons and there is no improvement in electronic conductivity. For example, Kolodiazhnyi and Petric[28] found that TiO_2 and niobium oxide second phases were formed when sintering the $Sr_{1-x/2}Ti_{1-x}Nb_xO_3$ ($x = 0.17$) at low oxygen partial pressure and high temperature. This transformation can be expressed with the following equation:

$$Sr_{1-\frac{x}{2}}Ti_{1-x}Nb_xO_3 \rightarrow Sr_{1-\frac{x}{2}}Ti_{1-x-y}Nb_{x-y}O_{3-4y} + yTiO_2 + yNbO_2, \quad (1)$$

where $y < x \leqslant 0.2$.

Furthermore, they observed a very high electronic conductivity of $Sr_{0.9}Ti_{0.8}Nb_{0.2}O_3$ and $Sr_{0.88}Y_{0.08}TiO_3$ when these samples were sintered in forming gas.[28]

In contrast to *n*-type doping, *p*-type dopants create an effective negative charge in the lattice. One way to neutralize the charge is introducing oxygen vacancies in the lattice. This mechanism of charge neutralization can take place at moderate oxygen chemical potentials and does generally not lead to improved electronic conductivity since there is no transfer of charges or electrons into the lattice. However, lowering the oxygen chemical potential can result in more oxygen vacancies, leading to an excess electron density in the lattice. The reduction reaction takes place at the surface of the material and delivers electrons to the lattice,[36]

$$O_O^{\times} \rightleftharpoons \tfrac{1}{2}O_2(g) + V_O^{\circ\circ} + 2e'. \quad (2)$$

These conduction electrons can often be transferred to neighboring atoms such as Ti, which can be mixed-valent Ti^{3+}/Ti^{4+}. As a result, the electrical conductivity of the material is again improved.

The addition of *p*-type impurities not only improves the electronic conductivity but also enhances the ionic conductivity by increasing the reducibility and number of oxygen vacancies in the material. Furthermore, the amount of available oxygen vacancies plays an essential role in the enhancement of the oxide ion diffusivity (D_{O_2}) in the lattice as evidenced by the following equation:[37]

$$D_{O_2} = \beta[V_{\ddot{O}}]a^2\nu_0 e^{-\Delta H_m/RT}, \quad (3)$$

where $[V_{\ddot{O}}]$ is the concentration of mobile vacancies; a is the cell parameter; ν_0 is a characteristic lattice frequency; ΔH_m is the enthalpy of vacancy migration; T is temperature; R is the ideal gas constant; and $\beta = \frac{z}{6} f e^{\Delta S_m/R}$ is a function of the number of equivalent near-neighbor sites z, the entropy of ion migration ΔS_m, and a correction factor f ($\approx$1). It is noted that the mobile vacancy concentration is usually smaller than the stoichiometric concentration due to vacancy trapping or vacancy ordering.[38,39]

Recently, various research groups reported that the catalytic activity and mixed ionic/electronic conductivity of *n*-type doped $SrTiO_3$ can be modified by B-site doping with *p*-type impurities such as Sc, Mn, and Ga.[40] For example, Li *et al.*[41,42] suggested that doping with Sc and Co at the B-site of $La_{0.3}Sr_{0.7}TiO_3$ can improve its ionic conductivity. Similarly, Xiao *et al.*[43] and Neagu and Irvine[44] proposed a similar doping strategy to improve the conductivity of *n*-type doped $SrTiO_3$ by enhancing bulk oxide ion mobility. In particular, they studied the effects of Ga dopants on the reducibility and conductivity of *n*-type doped $SrTiO_3$ systems by varying the concentration of Ga. They found that Ga doping promotes fast reduction and improves the phase stability of the material in an oxidizing environment. Impressive improvements in total conductivity were observed when doping with small amounts of Ga.

It is the objective of this theoretical study to further investigate the effect of concurrent *n*- and *p*-doping on the number of oxygen vacancies and the electronic conductivity of $SrTiO_3$ perovskites. In particular, we performed density functional theory (DFT) calculations of Nb- and Ga-doped $SrTiO_3$ and analyzed the electronic structure of the resulting materials. To evaluate the thermodynamic stability of doped $SrTiO_3$ phases at synthesized and anodic SOFC conditions, we furthermore performed constrained *ab initio* thermodynamic simulations.

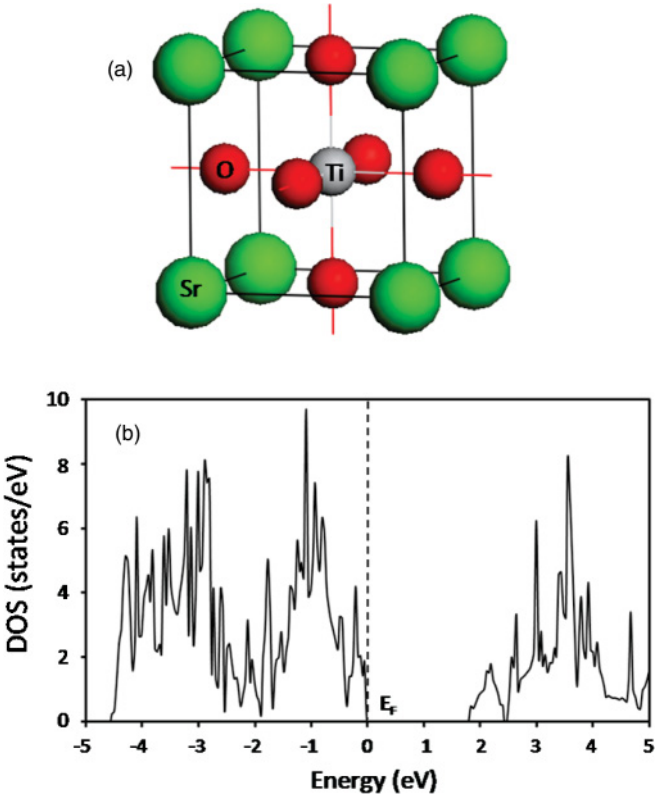

FIG. 1. (Color online) (a) Unit cell of $SrTiO_3$ perovskite oxide. (b) Density of states of stoichiometric $SrTiO_3$ with calculated band gap of 1.80 eV.

II. COMPUTATIONAL DETAILS

A. Crystallographic data of $SrTiO_3$

Stoichiometric $SrTiO_3$ develops an ideal cubic perovskite structure at room temperature with $Pm3m$ space group. The structural phase transition from cubic to tetragonal and to orthorhombic occurs at 110 and 65 K, respectively.[45] The cubic unit cell includes one molecular unit of $SrTiO_3$. As shown in Fig. 1(a), the structure contains 12-coordinated strontium ions occupying corner positions of the cube, whereas the titanium ion, at the center of the cubic cell, is surrounded by six oxygen ions forming a TiO_6 octahedral unit. The octahedral units are connected by a sharing Ti–O–Ti bridge, forming a three-dimensional framework.

B. Computational method

To investigate the bulk electronic properties of stoichiometric and doped $SrTiO_3$, we initially optimized the lattice parameter of the $SrTiO_3$ unit cell and created a 100 atom supercell containing twenty unit cells ($5 \times 2 \times 2$). To generate doped structures we replaced B-site cations (Ti) with various amounts of *n*-type (Nb) and *p*-type (Ga) dopants. Substitution of two Ti atoms with two dopants yields 10% B-site doped $SrTiO_3$, etc. In order to better understand the charge compensation mechanism in *n*- and *p*-type doped systems, both A-site deficient and reduced structures were created by generating strontium vacancies and

oxygen vacancies, respectively. In this study we considered up to two strontium vacancies and three oxygen vacancies in each structure. For all doped structures, we employed the lattice parameter of 20% Nb-doped $SrTiO_3$ and tried close to all ion position possibilities to identify the lowest energy structures.

All calculations performed for this study are based on the plane wave DFT implementation of the Vienna Ab initio Simulation Package (VASP 4.6).[46,47] We used the projector-augmented wave (PAW) method to represent the inner core potentials[46] and treated the Sr $4s4p5s$, Ti $3d4s$, O $2s2p$, Nb $4p5s4d$, and Ga $4s4p$ as valence electrons. The cutoff of the kinetic energy was set for all calculations to 400 eV. Exchange correlation is described within the generalized gradient approximation (GGA) with the Perdew-Burke-Ernzerhof (PBE) functional.[48] All calculations are spin-polarized, and Brillouin zone integration was performed with a $2 \times 5 \times 5$ Monkhorst-Pack k-point mesh.[49] For density of state (DOS) calculations we used a $4 \times 10 \times 10$ k-mesh. In all structure optimizations, all atoms are fully relaxed until the Hellman-Feynman forces are less than 0.02 eV $Å^{-1}$.

Our calculated stoichiometric $SrTiO_3$ bulk unit cell has an optimized lattice constant of 3.948 Å, which is in reasonable agreement to the experimental value of 3.90 Å.[50] The optimized supercell of 20% Nb-doped $SrTiO_3$ exhibits only a very small change in lattice parameters (3.949 Å) to that of stoichiometric $SrTiO_3$. Computations predict a Sr-O and Ti-O bond distance of 2.792 and 1.974 Å, respectively. As illustrated in Fig. 1(b), the DOS of stoichiometric $SrTiO_3$ exhibits insulating behavior with a band gap of 1.80 eV. It should be noted that while DFT within the GGA approximation is known to underestimate band gaps, several studies showed excellent agreement in the predicted electronic behavior of doped oxides computed by DFT within the GGA approximation and experimental observation.[51–53]

III. RESULTS AND DISCUSSION

In this work we are most interested in the electronic properties of *n*- and *p*-type doped $SrTiO_3$. Kolodiazhnyi and Petric[28] observed experimentally that $Sr_{0.9}Ti_{0.8}Nb_{0.2}O_3$ exhibits a very high conductivity at low oxygen chemical potential, and Xiao *et al.*[43] suggested that the reducibility of this material can be promoted by doping with a certain (small) amount of *p*-type dopant (Ga). Therefore, we performed three different sets of calculations based on the concentration of B-site dopants, i.e., 20% Nb-doped $SrTiO_3$, 10% Ga- and 20% Nb-doped $SrTiO_3$, and 20% Ga- and 20% Nb-doped $SrTiO_3$. In this way we can systematically study the effect of Ga (*p*-type) doping on Nb (*n*-type) doped $SrTiO_3$ on the reducibility/phase stability and electronic conductivity/DOS of the resulting materials.

For all structures we first performed constrained *ab initio* thermodynamic calculations to evaluate the relative thermodynamic stability of the systems. This *ab initio* thermodynamic approach allows us to calculate the free energy of different systems as a function of oxygen chemical potential, i.e., temperature and oxygen partial pressure, and to construct phase diagrams. The reaction energies of the most dominant structures in the phase diagrams are summarized in Table I. Next, the DOS related to the most dominant structures in the phase diagram were evaluated and analyzed with respect to the relative electronic conductivity. Figures of all structures found most stable at a specific oxygen chemical potential and the stoichiometry and reaction energy of all structures considered can be found in the supporting information.[54]

TABLE I. Summary of reaction energies used in constrained *ab initio* thermodynamic calculations.

Phase diagram	Reaction	ΔE (eV)
Nb_2O_5/NbO_2	$Nb_2O_5 \rightarrow 2NbO_2 + 1/2O_2$	3.71
20% Nb-doped	$Sr_{20}Ti_{16}Nb_4O_{60} + 1/2O_2 \rightarrow Sr_{19}Ti_{16}Nb_4O_{60} + SrO$	−1.94
$SrTiO_3$ with SrO-rich phase	$Sr_{20}Ti_{16}Nb_4O_{60} + O_2 \rightarrow Sr_{18}Ti_{16}Nb_4O_{60} + 2SrO$	−3.49
20% Nb-doped	$19Sr_{18}Ti_{16}Nb_4O_{60} \rightarrow 18Sr_{19}Ti_{16}Nb_4O_{60} + 16TiO_2 + 2Nb_2O_5 + 9O_2$	2.58
$SrTiO_3$ with	$10Sr_{18}Ti_{16}Nb_4O_{60} \rightarrow 9Sr_{20}Ti_{16}Nb_4O_{60} + 16TiO_2 + 2Nb_2O_5 + 9O_2$	5.24
TiO_2/niobium oxide-	$19Sr_{18}Ti_{16}Nb_4O_{60} \rightarrow 18Sr_{19}Ti_{16}Nb_4O_{60} + 16TiO_2 + 4NbO_2 + 10O_2$	2.97
rich phases	$10Sr_{18}Ti_{16}Nb_4O_{60} \rightarrow 9Sr_{20}Ti_{16}Nb_4O_{60} + 16TiO_2 + 4NbO_2 + 10O_2$	5.98
10% Ga- and 20%	$Sr_{20}Ti_{14}Nb_4Ga_2O_{60} + 1/2O_2 \rightarrow Sr_{19}Ti_{14}Nb_4Ga_2O_{60} + SrO$	−1.74
Nb-doped $SrTiO_3$	$Sr_{20}Ti_{14}Nb_4Ga_2O_{60} \rightarrow Sr_{20}Ti_{14}Nb_4Ga_2O_{59} + 1/2O_2$	4.54
with	$Sr_{20}Ti_{14}Nb_4Ga_2O_{60} \rightarrow Sr_{20}Ti_{14}Nb_4Ga_2O_{58} + O_2$	9.01
SrO-rich phase	$Sr_{20}Ti_{14}Nb_4Ga_2O_{60} \rightarrow Sr_{20}Ti_{14}Nb_4Ga_2O_{57} + 3/2O_2$	14.16
10% Ga- and	$19Sr_{18}Ti_{14}Nb_4Ga_2O_{60} \rightarrow 18Sr_{19}Ti_{14}Nb_4Ga_2O_{60} + 14TiO_2 + 2Nb_2O_5 + Ga_2O_3 + 19/2O_2$	−1.29
20% Nb-doped	$10Sr_{18}Ti_{14}Nb_4Ga_2O_{60} \rightarrow 9Sr_{20}Ti_{14}Nb_4Ga_2O_{60} + 14TiO_2 + 2Nb_2O_5 + Ga_2O_3 + 19/2O_2$	1.28
$SrTiO_3$ with	$10Sr_{18}Ti_{14}Nb_4Ga_2O_{60} \rightarrow 9Sr_{20}Ti_{14}Nb_4Ga_2O_{59} + 14TiO_2 + 2Nb_2O_5 + Ga_2O_3 + 14O_2$	5.37
TiO_2/Ga_2O_3/niobium	$10Sr_{18}Ti_{14}Nb_4Ga_2O_{60} \rightarrow 9Sr_{20}Ti_{14}Nb_4Ga_2O_{58} + 14TiO_2 + 2Nb_2O_5 + Ga_2O_3 + 37/2O_2$	9.39
oxide-rich phases	$10Sr_{18}Ti_{14}Nb_4Ga_2O_{60} \rightarrow 9Sr_{20}Ti_{14}Nb_4Ga_2O_{57} + 14TiO_2 + 2Nb_2O_5 + Ga_2O_3 + 23O_2$	14.03
20% Ga- and	$10Sr_{18}Ti_{12}Nb_4Ga_4O_{60} \rightarrow 9Sr_{20}Ti_{12}Nb_4Ga_4O_{60} + 12TiO_2 + 2Nb_2O_5 + 2Ga_2O_3 + 10O_2$	−2.81
20% Nb-doped	$10Sr_{18}Ti_{12}Nb_4Ga_4O_{60} \rightarrow 9Sr_{20}Ti_{12}Nb_4Ga_4O_{59} + 12TiO_2 + 2Nb_2O_5 + 2Ga_2O_3 + 29/2O_2$	1.21
$SrTiO_3$	$10Sr_{18}Ti_{12}Nb_4Ga_4O_{60} \rightarrow 9Sr_{20}Ti_{12}Nb_4Ga_4O_{58} + 12TiO_2 + 2Nb_2O_5 + 2Ga_2O_3 + 19O_2$	5.21
	$10Sr_{18}Ti_{12}Nb_4Ga_4O_{60} \rightarrow 9Sr_{20}Ti_{12}Nb_4Ga_4O_{57} + 12TiO_2 + 2Nb_2O_5 + 2Ga_2O_3 + 47/2O_2$	9.82

A. Electronic structure and phase diagram of 20% Nb-doped $SrTiO_3$

In this set of calculations we substituted four Ti atoms with four Nb atoms in the $5 \times 2 \times 2$ supercell to obtain a model for 20% Nb-doped $SrTiO_3$ ($Sr_{20}Ti_{16}Nb_4O_{60}$ or $SrTi_{0.8}Nb_{0.2}O_3$). In addition we generated structures with one or two Sr vacancies to create partial (5%) A-site deficient ($Sr_{19}Ti_{16}Nb_4O_{60}$ or $Sr_{0.95}Ti_{0.8}Nb_{0.2}O_3$) and full (10%) A-site deficient 20% Nb-doped $SrTiO_3$ ($Sr_{18}Ti_{16}Nb_4O_{60}$ or $Sr_{0.9}Ti_{0.8}Nb_{0.2}O_3$) model structures, respectively. From the configuration of the most stable structures, we observe that Nb impurities prefer to be as far apart as possible due to the repulsion of the extra electrons from the Nb^{5+} cations that can be transferred to neighboring Ti atoms that are mixed-valent Ti^{3+}/Ti^{4+}. In contrast when there are Sr vacancies in the structure, Nb prefers to stay close to the vacancies since the charges originating from the Nb atoms can be compensated by the absence of the Sr^{2+} cations. Moreover, it was found that the Sr-vacancy sites stay apart from each other in structures with more than one vacancy (see supplementary material for the structures, Fig. S1).[54]

Constrained *ab initio* thermodynamic calculations of 20% Nb-doped $SrTiO_3$ systems were performed to determine the phase stability of these structures at various temperatures and oxygen partial pressures. We employed two different types of calculations based on the main products that were generated when the phase transition occurred. First, we calculated the free energies of 20% Nb-doped $SrTiO_3$ with a SrO-rich second phase experimentally obtained by cooling $SrTi_{0.8}Nb_{0.2}O_3$,

$$Sr_{20}Ti_{16}Nb_4O_{60} + \frac{x}{2}O_2 \rightarrow Sr_{20-x}Ti_{16}Nb_4O_{60} + xSrO, \quad (4)$$

where x represents the number of Sr-vacancy sites in the structure ($x = 1,2$), and free energies are given by

$$\Delta G = E_{\mathrm{Sr-vacancy}} + xE_{\mathrm{SrO}} - E_{\mathrm{full}} - x[E_{\mathrm{O}} + \Delta\mu_O(T,P)], \quad (5)$$

with $E_{\mathrm{Sr-vacancy}}$ being the DFT-calculated electronic energy of the structure with Sr-vacancy, E_{full} is the DFT-calculated electronic energy of the structure without Sr-vacancy, E_{SrO} is the DFT-calculated electronic energy of the SrO lattice, and E_{O} is half of the energy of an oxygen molecule $E_{\mathrm{O_2}}$, which is obtained from the H_2O splitting reaction using the experimental reaction energy and calculated DFT energies of H_2 and H_2O in the gas phase,[55,56]

$$E_{\mathrm{O_2}} = 2\left[\left(E^{\mathrm{DFT}}_{\mathrm{H_2O}} + E^{\mathrm{ZPE}}_{\mathrm{H_2O}}\right) - \left(E^{\mathrm{DFT}}_{\mathrm{H_2}} + E^{\mathrm{ZPE}}_{\mathrm{H_2}}\right) - E_{\mathrm{hof}}\right] - E^{\mathrm{ZPE}}_{\mathrm{O_2}}, \quad (6)$$

where E^{ZPE} is the experimental zero point energy,[57] E_{hof} is the experimental heat of formation of a gas-phase H_2O molecule,[57] and E^{DFT} is the energy calculated with PBE functional. The chemical potential of O, which includes the temperature- and pressure-dependent free energy contributions of the O_2 molecule, is described by $\Delta\mu_O(T,P)$ and has been calculated from first principles and the rotational, translational, and vibrational partition functions of the O_2 molecule. We note that we neglect all zero point energies in Eq. (5) and assume that entropic contributions from the solids to the free energy difference are insignificant.[58–60] Also, the pressure dependence of $\Delta\mu_O(T,P)$ is obtained assuming that the gas phase is ideal,[59]

$$\Delta\mu_O(T,P) = \frac{1}{2}\left(\Delta\mu_{O_2}(T,P^0) + k_BTln\left(\frac{P}{P^0}\right)\right). \quad (7)$$

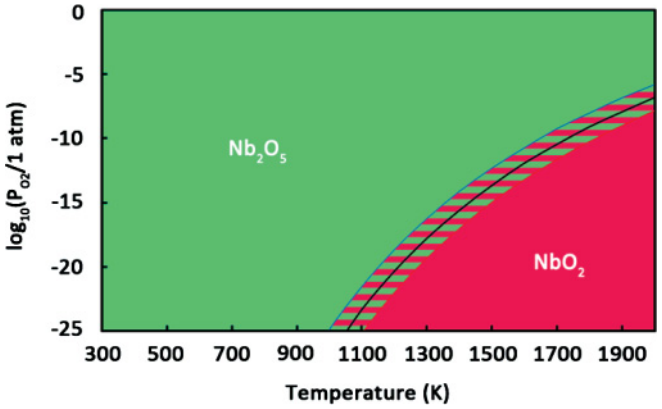

FIG. 2. (Color online) Calculated phase diagram of Nb_2O_5/NbO_2. Differently shaded areas mark the stability regions of various structures for a given temperature and partial pressure of oxygen. The hatched area decribes possible changes in the phase diagram if computed reaction energies shown in Table I are off by ± 0.2 eV (our estimated error bar). Green and red areas symbolize stability of Nb_2O_5 and NbO_2, respectively.

Next, we employed the same *ab initio* thermodynamic approach to investigate the thermodynamic stability of 20% Nb-doped $SrTiO_3$ with TiO_2 and niobium oxide-rich second phases that can experimentally be obtained by heating Sr-deficient 20% Nb-doped $SrTiO_3$. Considering that Nb_2O_5 can be reduced to NbO_2 in a reducing environment at high temperature,[61] we first performed *ab initio* thermodynamic calculations of the Nb_2O_5/NbO_2 system

$$Nb_2O_5 \rightarrow 2NbO_2 + \tfrac{1}{2}O_2, \quad (8)$$

and Fig. 2 illustrates that at low temperature Nb_2O_5 is the dominant phase whereas the NbO_2 phase predominates at higher temperatures.

In the following we performed *ab initio* thermodynamic calculations of the Nb-doped $SrTiO_3$ system according to the dominant phase in the Nb_2O_5/NbO_2 phase diagram, i.e., whenever the Nb_2O_5 phase is preferred we calculate the free energies of the system according to Eq. (9),

$$(20-x)Sr_{18}Ti_{16}Nb_4O_{60} \rightarrow 18Sr_{20-x}Ti_{16}Nb_4O_{60} + (32-16x)TiO_2 + (4-2x)Nb_2O_5 + (18-9x)O_2 \quad (9)$$

and whenever NbO_2 is preferred, we calculate the free energies of the system according to Eq. (10),

$$(20-x)Sr_{18}Ti_{16}Nb_4O_{60} \rightarrow 18Sr_{20-x}Ti_{16}Nb_4O_{60} + (32-16x)TiO_2 + (8-4x)NbO_2 + (20-10x)O_2, \quad (10)$$

where x is the number of Sr vacancies with $x = 0,1$. Figure 3 shows the calculated phase diagrams of 20%

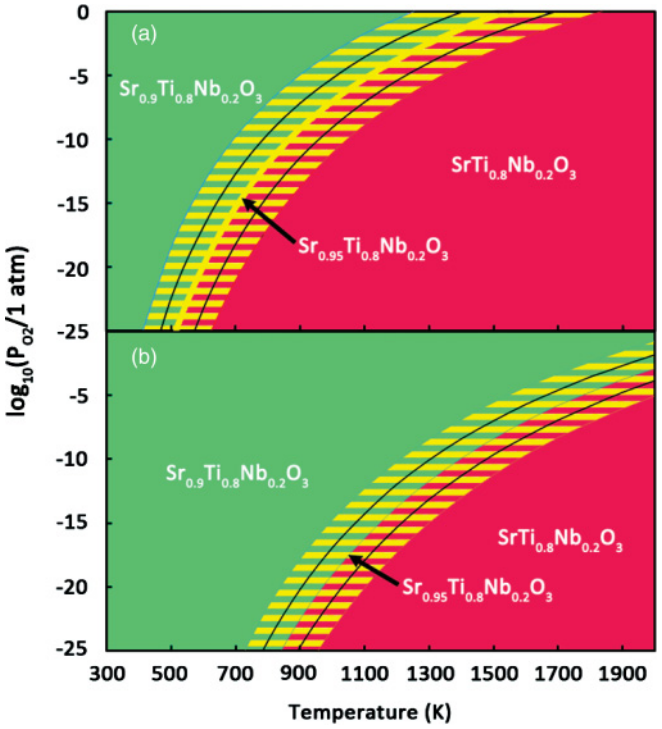

FIG. 3. (Color online) Calculated phase diagram of 20% Nb-doped $SrTiO_3$ with (a) SrO-rich phase and (b) TiO_2/niobium oxide-rich phases. Differently shaded areas mark the stability regions of various structures for a given temperature and partial pressure of oxygen. The hatched area decribes possible changes in the phase diagram if computed reaction energies shown in Table I are off by ±0.2 eV (our estimated error bar). Green, yellow, and red areas symbolize stability of $Sr_{0.9}Ti_{0.8}Nb_{0.2}O_3$, $Sr_{0.95}Ti_{0.8}Nb_{0.2}O_3$, and $SrTi_{0.8}Nb_{0.2}O_3$, respectively.

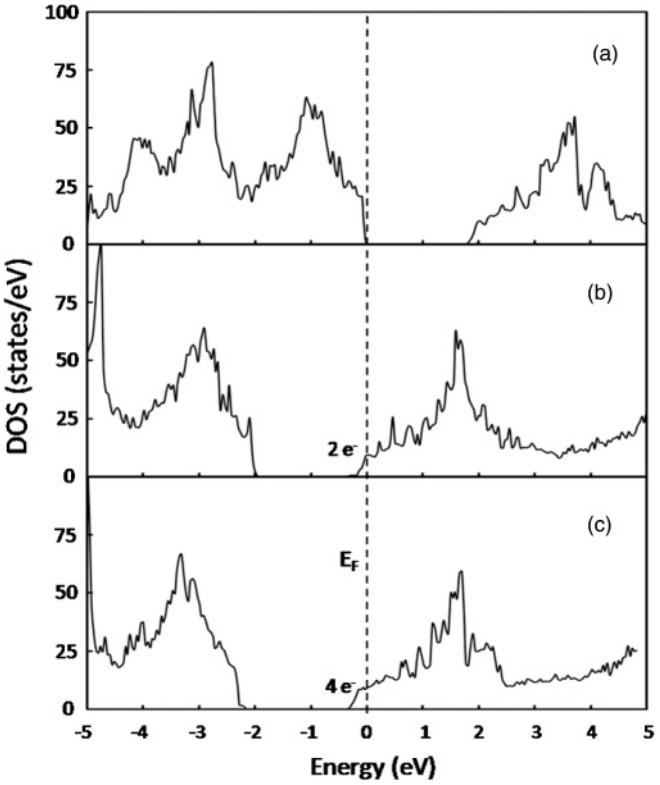

FIG. 4. Density of states of (a) $Sr_{0.9}Ti_{0.8}Nb_{0.2}O_3$, (b) $Sr_{0.95}Ti_{0.8}Nb_{0.2}O_3$, and (c) $SrTi_{0.8}Nb_{0.2}O_3$. Fermi energy is set to zero on energy scale. Numbers of electrons shown in the figure indicate the integrated number of electrons per supercell for the specified DOS area, i.e., states below the Fermi level.

Nb-doped $SrTiO_3$ with SrO-rich second phase and TiO_2 and niobium oxide-rich second phases. The phase transformation from 10% Sr-deficient ($Sr_{0.9}Ti_{0.8}Nb_{0.2}O_3$) to 5% Sr-deficient ($Sr_{0.95}Ti_{0.8}Nb_{0.2}O_3$) to non-Sr-deficient structures ($SrTi_{0.8}Nb_{0.2}O_3$) occurs with increasing temperature and decreasing oxygen partial pressure. We note that an oxygen deficient structure is thermodynamically unstable in the considered temperature and oxygen partial-pressure range.

The electronic conductivity of these materials can, to a first approximation, be analyzed from their electronic structures. As illustrated in Fig. 4(a), the DOS of a 10% Sr-deficient material ($Sr_{0.9}Ti_{0.8}Nb_{0.2}O_3$) exhibits insulating behavior with a band gap of 1.80 eV. The charges from the four Nb dopants are compensated by the presence of two Sr vacancies. The DOS of the 5% Sr-deficient structure ($Sr_{0.95}Ti_{0.8}Nb_{0.2}O_3$) shows a slight improvement in electronic conductivity [Fig. 4(b)]. The Fermi energy shifts inside the conduction band with two conduction electrons per supercell below the Fermi level. An even greater improvement in the electronic conductivity occurs when the material is fully electronically compensated. As depicted in Fig. 4(c), the DOS of 20% Nb-doped $SrTiO_3$ with no Sr vacancies ($SrTi_{0.8}Nb_{0.2}O_3$) exhibits metallic character with four delocalized electrons at the Fermi level. Calculated band structures of this material shown in the supporting information (Fig. S5) confirm the metallic behavior of this material.[54]

It is interesting to note that the simulation results are in agreement with experimental observations from Kolodiazhnyi and Petric.[28] They reported that the transformation of cation vacancy compensated materials to electronically compensated materials (and corresponding change in electronic conductivity) occurred when the materials were equilibrated at high temperature and low oxygen partial pressure. This condition corresponds to anodic SOFC conditions with temperatures between 1000 and 1200 K and oxygen partial pressures in the range of 10^{-20} bar.

B. Electronic structure and phase diagram of 10% Ga- and 20% Nb-doped $SrTiO_3$

Substitution of two Ti atoms with two Ga atoms in our 20% Nb-doped $SrTiO_3$ model leads to 10% Ga- and 20% Nb-doped $SrTiO_3$. The presence of Sr and oxygen vacancies in the structure was investigated in a similar manner, as described previously. It is found that Ga atoms prefer to be next to Nb atoms since the extra electron from the Nb dopant can be compensated by the electron hole generated from the Ga dopant (see also supporting information, Fig. S2).[54] At high temperatures and low oxygen partial pressure oxygen vacancies start to form. The first oxygen vacancy is created by removing an oxygen atom from the Ga–O–Ti bridge forming GaO_5 units, whereas the second vacancy is positioned next to the same Ga atom generating a GaO_4 unit. Upon removal of the third oxygen atom another GaO_5 unit is formed in our unit

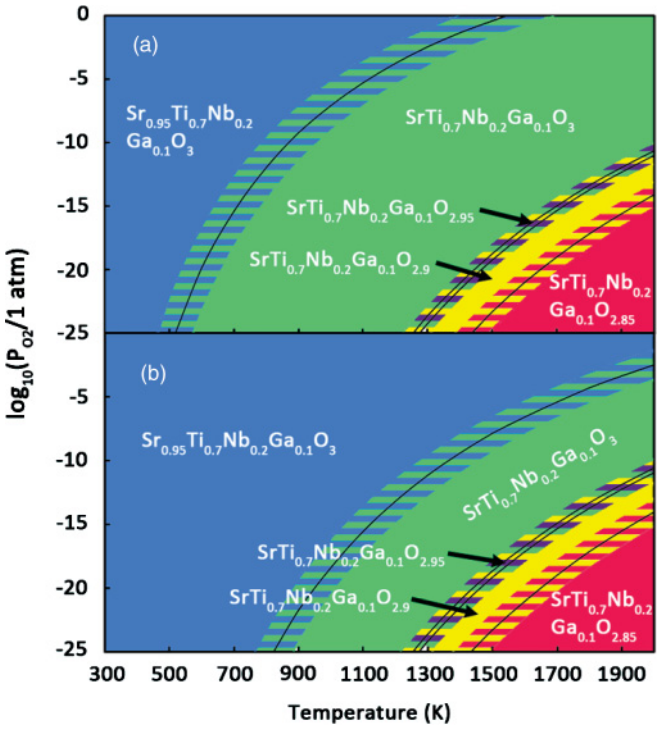

FIG. 5. (Color online) Calculated phase diagram of 10% Ga- and 20% Nb-doped $SrTiO_3$ with (a) SrO-rich phase and (b) TiO_2/Ga_2O_3/niobium oxide-rich phases. Differently shaded areas mark the stability regions of various structures for a given temperature and partial pressure of oxygen. The hatched area decribes possible changes in the phase diagram if computed reaction energies shown in Table I are off by ±0.2 eV (our estimated error bar). Blue, green, yellow, and red areas symbolize stability of $Sr_{0.95}Ti_{0.7}Nb_{0.2}Ga_{0.1}O_3$, $SrTi_{0.7}Nb_{0.2}Ga_{0.1}O_3$, $SrTi_{0.7}Nb_{0.2}Ga_{0.1}O_{2.9}$, and $SrTi_{0.7}Nb_{0.2}Ga_{0.1}O_{2.85}$, respectively. The hatched violet area symbolizes the possible stability of a $SrTi_{0.7}Nb_{0.2}Ga_{0.1}O_{2.95}$ phase.

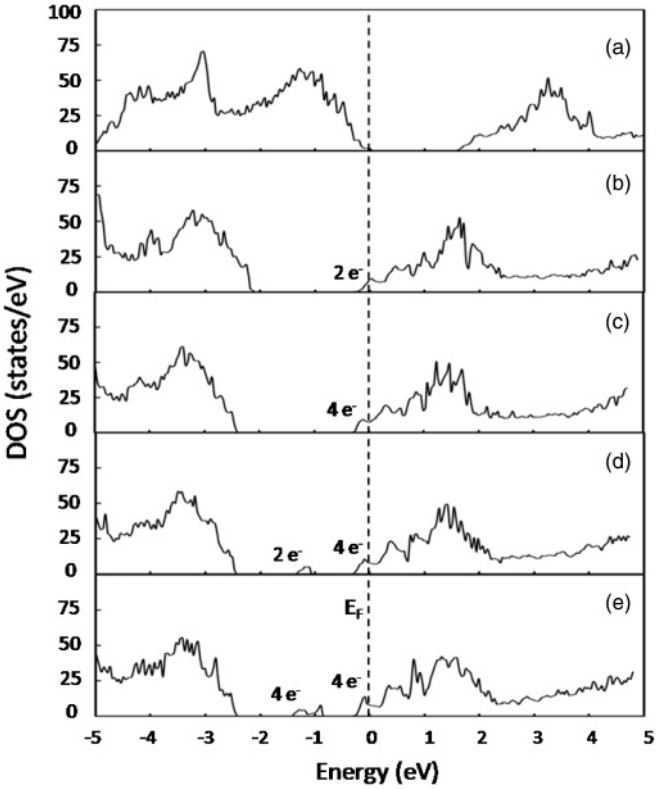

FIG. 6. Density of states of (a) $Sr_{0.95}Ti_{0.7}Nb_{0.2}Ga_{0.1}O_3$, (b) $SrTi_{0.7}Nb_{0.2}Ga_{0.1}O_3$, (c) $SrTi_{0.7}Nb_{0.2}Ga_{0.1}O_{2.95}$, (d) $SrTi_{0.7}Nb_{0.2}Ga_{0.1}O_{2.9}$, and (e) $SrTi_{0.7}Nb_{0.2}Ga_{0.1}O_{2.85}$. Fermi energy is set to zero on energy scale. Numbers of electrons shown in the figure indicate the integrated number of electrons per supercell for the specified DOS area, i.e., states in the band gap and states below the Fermi level.

cell. It is noteworthy that we find structures with neighboring Ga atoms to be significantly less stable.

Figures 5(a) and 5(b) illustrate the phase diagram for 10% Ga- and 20% Nb-doped $SrTiO_3$ as a function of temperature and partial pressure of oxygen corresponding to the formation of SrO and TiO_2/Ga_2O_3/niobium oxide-rich second phases, respectively. In the presence of Ga we find that the reduced structures ($SrTi_{0.7}Nb_{0.2}Ga_{0.1}O_{2.95}$, $SrTi_{0.7}Nb_{0.2}Ga_{0.1}O_{2.90}$, and $SrTi_{0.7}Nb_{0.2}Ga_{0.1}O_{2.85}$) are stable in the studied high temperature and low oxygen partial pressure range. The existence of a reduced structure indicates that Ga doping improves the reducibility of the materials, as previously reported in Neagu and Irvine's work.[44] More interestingly, Ga and Nb dopants do not seem to compensate each other with respect to electronic conductivity. Figure 6 illustrates the DOS of the most important structures. While $Sr_{0.95}Ti_{0.7}Nb_{0.2}Ga_{0.1}O_3$ exhibits insulating behavior with a band gap of 1.80 eV (the charges from the Nb dopants are compensated by the Sr vacancies and Ga dopants), $SrTi_{0.7}Nb_{0.2}Ga_{0.1}O_3$, $SrTi_{0.7}Nb_{0.2}Ga_{0.1}O_{2.95}$, $SrTi_{0.7}Nb_{0.2}Ga_{0.1}O_{2.90}$, and $SrTi_{0.7}Nb_{0.2}Ga_{0.1}O_{2.85}$ exhibit metallic behavior with up to four conduction electrons at the Fermi level (the same number as in the absence of Ga). In $SrTi_{0.7}Nb_{0.2}Ga_{0.1}O_3$, the two Ga atoms in the supercell compensate for two of the Nb atoms, leaving the remaining two Nb atoms to contribute two conduction electrons at the Fermi level [Fig. 6(b)]. In $SrTi_{0.7}Nb_{0.2}Ga_{0.1}O_{2.95}$, one oxygen atom connected to a Ga atom is removed, compensating the hole doping effect of two Ga atoms. Thus, we see the effect of 20% Nb doping in this structure [Fig. 6(c)]. In $SrTi_{0.7}Nb_{0.2}Ga_{0.1}O_{2.9}$ and $SrTi_{0.7}Nb_{0.2}Ga_{0.1}O_{2.85}$, the electrons generated by creating further oxygen vacancies are localized mainly on the Ga atoms, and an extra peak is observed in the DOS [Figs. 6(d) and 6(e)] between the valence band and the conduction band. A partial density of states (PDOS) analysis and electron density integration for $SrTi_{0.7}Nb_{0.2}Ga_{0.1}O_{2.9}$, as illustrated in Fig. 7(a), shows that there are two electrons in this peak, which predominantly contains contributions from the oxygen PDOS. We see no reason for these two electrons to be delocalized and believe that these states do not contribute to the electronic conductivity of the material. We find a qualitatively similar picture for the four electrons in the extra peak in the band gap of $SrTi_{0.7}Nb_{0.2}Ga_{0.1}O_{2.85}$. This observation is in agreement with previous computational and experimental results that the electrons from oxygen vacancies are often localized and have little contribution to the electronic conductivity of the materials.[62,63] Next, Fig. 7(b) shows the PDOS of $SrTi_{0.7}Nb_{0.2}Ga_{0.1}O_{2.9}$ below the Fermi level and confirms that these states are primarily from mixed-valent Ti^{3+}/Ti^{4+} that contribute to electronic conduction. A similar

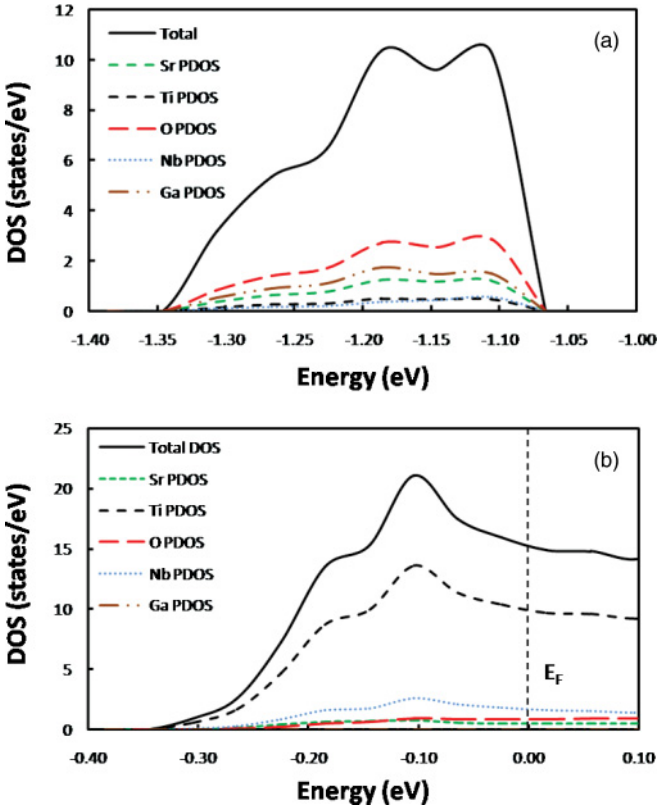

FIG. 7. (Color online) Partial density of states of (a) the gap states between the valence and conduction band and (b) the states below the Fermi level in $SrTi_{0.7}Nb_{0.2}Ga_{0.1}O_{2.9}$.

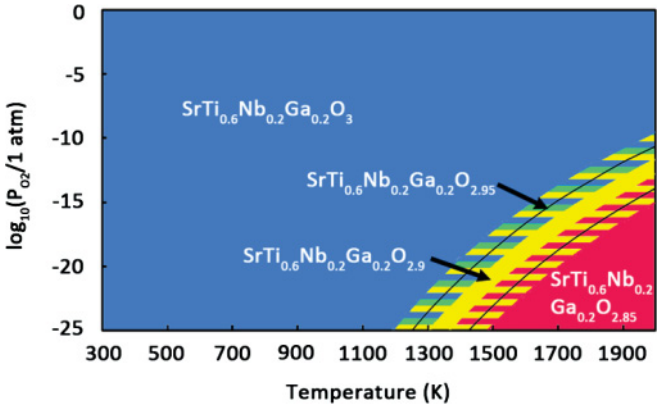

FIG. 8. (Color online) Calculated phase diagram of 20% Ga- and 20% Nb-doped $SrTiO_3$. Differently shaded areas mark the stability regions of various structures for a given temperature and partial pressure of oxygen. The hatched area decribes possible changes in the phase diagram if computed reaction energies shown in Table I are off by ±0.2 eV (our estimated error bar). Blue, yellow, and red areas symbolize stablity of $SrTi_{0.6}Nb_{0.2}Ga_{0.2}O_3$, $SrTi_{0.6}Nb_{0.2}Ga_{0.2}O_{2.9}$, and $SrTi_{0.6}Nb_{0.2}Ga_{0.2}O_{2.85}$, respectively. The hatched green area symbolizes the stability of a $SrTi_{0.6}Nb_{0.2}Ga_{0.2}O_{2.95}$ phase.

behavior is observed for all structures studied with states below the Fermi level.

To conclude, further doping of 20% Nb-doped $SrTiO_3$ with 10% Ga leads to a comparable degree of electronic conductivity to that of only 20% Nb-doped $SrTiO_3$ under anodic SOFC conditions. Further, Ga promotes ionic conductivity by enhancing the reducibility of the material. These results support the experimental observations reported by several groups[43,44] that Ga-doped titanates possess a high number of oxygen vacancies and good oxide-ion conduction.

C. Electronic structure and phase diagram of 20% Ga- and 20% Nb-doped $SrTiO_3$

Replacing another two Ti atoms with Ga atoms in 10% Ga- and 20% Nb-doped $SrTiO_3$ we obtain a model for 20% Ga- and 20% Nb-doped $SrTiO_3$. The most stable structures in this set of calculations have Ga atoms close to Nb atoms. Up to three oxygen vacancies were generated in this structure to study the effect of reducing conditions. It is preferable to create the first two oxygen vacancies at the Ga–O–Ti bridge where two vacancies share the same Ga atom forming a GaO_4 unit, whereas the third oxygen vacancy is again positioned at a Ga–O–Ti bridge forming a GaO_5 unit (see supporting information for the structures, Fig. S3).[54]

Constrained *ab initio* thermodynamic calculations of this system were carried out to determine the phase stability at various temperatures and oxygen partial pressures. In some respects the phase transition of this system is quite similar to that of the 10% Ga-doped system. In particular, the presence of a reduced phase of both the 10 and 20% Ga-doped systems occurs at approximately the same temperature and oxygen partial pressure range, indicating that increasing the concentration of Ga does not significantly improve the reducibility of the material. However, the phase diagram of the 20% Ga-doped system shown in Fig. 8 displays no Sr-deficient phase (i.e., there are no SrO or TiO_2/Ga_2O_3/niobium oxide-rich second phases). Furthermore, we observe from the DOS (Fig. 9) a reduction in the electronic conductivity with increase in Ga doping. As shown in Figs. 9(c) and 9(d), the DOS of $SrTi_{0.6}Nb_{0.2}Ga_{0.2}O_{2.9}$ and $SrTi_{0.6}Nb_{0.2}Ga_{0.2}O_{2.85}$ exhibit only two conduction electrons at the Fermi level. It seems that doping with 20% Ga (and 20% Nb) and removing the first oxygen atom in our supercell leads to a compensation of the hole-doping effect of two Ga atoms and generation of two conduction electrons from two uncompensated Nb atoms at the Fermi level [Fig. 9(b)]. In contrast, removing one or two more oxygen atoms from the supercell leads to localized electrons observed in an extra peak in the DOS between the valence and conduction band and no compensation of the hole-doping effect of the remaining two Ga atoms, and thus, no increase in charge carrier density [Figs. 9(c) and 9(d)]. Interestingly, creating a fourth oxygen vacancy under very reducing conditions (usually not encountered in SOFC operation and therefore not included in the phase diagram) leads again to a full compensation of the hole-doping effect of all four Ga atoms and generation of four conduction electrons from the four Nb atoms at the Fermi level (see supporting information, Fig. S4).[54] Thus, while doping with 20% Ga improves the ionic conductivity, the electronic conductivity of the material is likely diminished under realistic fuel cell operating conditions.

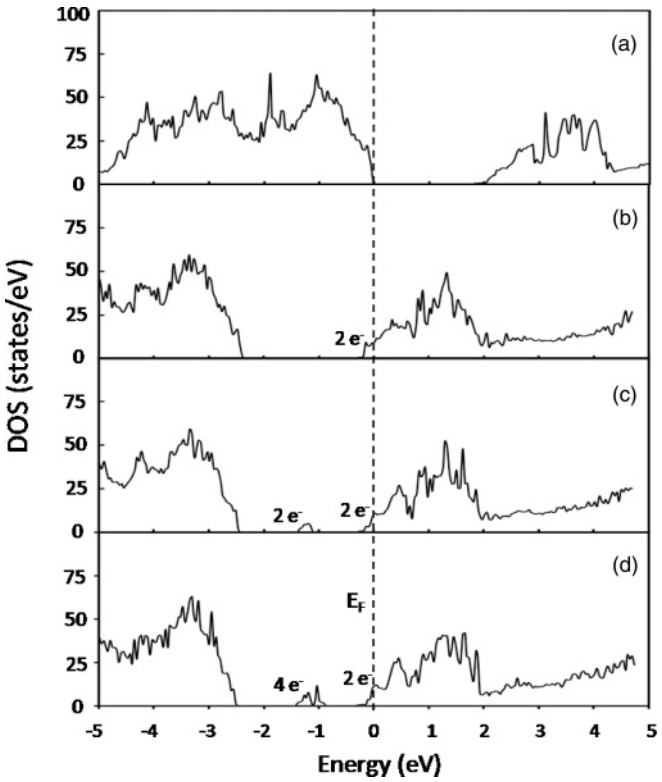

FIG. 9. Density of states of (a) $SrTi_{0.6}Nb_{0.2}Ga_{0.2}O_3$, (b) $SrTi_{0.6}Nb_{0.2}Ga_{0.2}O_{2.95}$, (c) $SrTi_{0.6}Nb_{0.2}Ga_{0.2}O_{2.9}$, and (d) $SrTi_{0.6}Nb_{0.2}Ga_{0.2}O_{2.85}$. Fermi energy is set to zero on the energy scale. Numbers of electrons shown in the figure indicate the integrated number of electrons per supercell for the specified DOS area, i.e., states in the band gap and states below the Fermi level.

IV. CONCLUSIONS

We have investigated the electronic properties and thermodynamic stability of Nb (*n*-type) and Ga (*p*-type) doped $SrTiO_3$ perovskites using DFT and constrained *ab initio* thermodynamic simulations. We find that cation vacancy compensated 20% Nb-doped Sr-deficient $SrTiO_3$ ($Sr_{0.9}Ti_{0.8}Nb_{0.2}O_3$) transforms to an electronically compensated non-Sr-deficient phase ($SrTi_{0.8}Nb_{0.2}O_3$) at high temperature and low oxygen partial pressure, which leads to a significant improvement in electronic conductivity. This result is in excellent agreement with the defect chemistry model and experimental observations reported by Kolodiazhnyi and Petric.[28] Doping 20% Nb-doped $SrTiO_3$ with 10% Ga enhances the ionic conductivity of the material by creating oxygen vacancies. The electronic conductivity is not reduced by small amounts of Ga so that a mixed ionic/electronic conductor is formed. However, doping with 20% Ga decreases the electronic conductivity of the material. This result supports the experimental observations[43,44] that doping with a small amount of Ga improves the conductivity and promotes fast reduction of the material. From both experimental observations and our calculations, we propose that a mixed *n*-type and *p*-type doping strategy could be a general approach to obtaining mixed ionic/electronic conductivity in perovskite oxide materials.

ACKNOWLEDGMENTS

Helpful discussions with Michele Pavone and Emily A. Carter at Princeton University are acknowledged. This work has been funded by the Heterogeneous Functional Materials Center (HeteroFoaM), an Energy Frontier Research Center funded by the US Department of Energy, Office of Basic Energy Sciences under Award No. DE-SC0001061. Computations were performed at the US Department of Energy facilities located at EMSL, a national scientific user facility located at Pacific Northwest National Laboratory (Grant Proposal No. 34900), at the National Energy Research Scientific Computing Center (NERSC), and at Oak Ridge National Laboratory (CNMS2009-248). Furthermore, a portion of this research was performed at Teragrid resources provided by the National Center for Supercomputing Applications (NCSA), Purdue University, and Texas Advanced Computing Center (TACC) under Grant No. TG-CTS090100. Finally, computing resources from the USC NanoCenter, USC's High Performance Computing Group, and the Minnesota Supercomputing Institute for Advanced Computational Research are gratefully acknowledged.

*Corresponding author:heyden@cec.sc.edu

[1]M. Guillodo, P. Vernoux, and J. Fouletier, Solid State Ionics **127**, 99 (2000).
[2]T. Iwata, J. Electrochem. Soc. **143**, 1521 (1996).
[3]A. Tsoga, A. Naoumidis, and P. Nikolopoulos, Acta Mater. **44**, 3679 (1996).
[4]D. Simwonis, F. Tietz, and D. Stover, Solid State Ionics **132**, 241 (2000).
[5]Y. B. Lin, Z. L. Zhan, and S. A. Barnett, J. Power Sources **158**, 1313 (2006).
[6]S. W. Tao and J. T. S. Irvine, Nature Materials **2**, 320 (2003).
[7]Y. H. Huang, R. I. Dass, Z. L. Xing, and J. B. Goodenough, Science **312**, 254 (2006).
[8]D. P. Fagg, V. V. Kharton, A. V. Kovalevsky, A. P. Viskup, E. N. Naumovich, and J. R. Frade, J. Eur. Ceram. Soc. **21**, 1831 (2001).
[9]S. Q. Hui and A. Petric, J. Eur. Ceram. Soc. **22**, 1673 (2002).
[10]T. Ishihara, H. Matsuda, and Y. Takita, J. Am. Chem. Soc. **116**, 3801 (1994).
[11]M. Feng and J. B. Goodenough, Eur. J. Solid State Inorg. Chem. **31**, 663 (1994).
[12]K. Q. Huang, M. Feng, J. B. Goodenough, and M. Schmerling, J. Electrochem. Soc. **143**, 3630 (1996).
[13]J. Canales-Vazquez, S. W. Tao, and J. T. S. Irvine, Solid State Ionics **159**, 159 (2003).
[14]O. A. Marina, N. L. Canfield, and J. W. Stevenson, Solid State Ionics **149**, 21 (2002).

[15] J. Canales-Vazquez, J. C. Ruiz-Morales, J. T. S. Irvine, and W. Z. Zhou, J. Electrochem. Soc. **152**, A1458 (2005).
[16] A. Sin, E. Kopnin, Y. Dubitsky, A. Zaopo, A. S. Arico, L. R. Gullo, D. La Rosa, and V. Antonucci, J. Power Sources **145**, 68 (2005).
[17] P. Vernoux, E. Djurado, and M. Guillodo, J. Am. Ceram. Soc. **84**, 2289 (2001).
[18] L. Aguilar, S. W. Zha, Z. Cheng, J. Winnick, and M. L. Liu, J. Power Sources **135**, 17 (2004).
[19] P. R. Slater, D. P. Fagg, and J. T. S. Irvine, J. Mater. Chem. **7**, 2495 (1997).
[20] J. A. Noland, Phys. Rev. **94**, 724 (1954).
[21] J. F. Schooley, W. R. Hosler, E. Ambler, J. H. Becker, M. L. Cohen, and C. S. Koonce, Phys. Rev. Lett. **14**, 305 (1965).
[22] Y. Aiura, H. Bando, I. Hase, S. Nishihara, Y. Haruyama, and H. Suzuki, Superlattices Microstruct. **21**, 321 (1997).
[23] N. Shanthi and D. D. Sarma, Phys. Rev. B **57**, 2153 (1998).
[24] T. Yokoya, T. Sato, H. Fujisawa, T. Takahashi, A. Chainani, and M. Onoda, Phys. Rev. B **59**, 1815 (1999).
[25] T. Jarlborg, Phys. Rev. B **61**, 9887 (2000).
[26] S. Lee, G. Kim, J. M. Vohs, and R. J. Gorte, J. Electrochem. Soc. **155**, B1179 (2008).
[27] H. Kurokawa, L. M. Yang, C. P. Jacobson, L. C. De Jonghe, and S. J. Visco, J. Power Sources **164**, 510 (2007).
[28] T. Kolodiazhnyi and A. Petric, J. Electroceram. **15**, 5 (2005).
[29] W. Luo, W. Duan, S. G. Louie, and M. L. Cohen, Phys. Rev. B **70**, 214109 (2004).
[30] U. Balachandran and N. G. Eror, J. Electrochem. Soc. **129**, 1021 (1982).
[31] A. M. J. Seuter, Philips Res. Repts 1 (1974).
[32] R. Moos and K. H. Hardtl, J. Am. Ceram. Soc. **80**, 2549 (1997).
[33] J. B. Goodenough and Y. H. Huang, J. Power Sources **173**, 1 (2007).
[34] R. Moos, A. Gnudi, and K. H. Härdtl, J. Appl. Phys. **78**, 5042 (1995).
[35] R. Moos, T. Bischoff, W. Menesklou, and K. H. Hardtl, J. Mater. Sci. **32**, 4247 (1997).
[36] M. J. Akhtar, Z. U. N. Akhtar, R. A. Jackson, and C. R. A. Catlow, J. Am. Ceram. Soc. **78**, 421 (1995).
[37] T. Ishihara (ed.), *Perovskite Oxide for Solid Oxide Fuel Cells* (Springer, New York, 2009), pp. 96–98.
[38] K. Vidyasagar, A. Reller, J. Gopalakrishnan, and C. N. R. Rao, J. Chem. Soc. Chem. Comm. 7 (1985).
[39] J. A. Kilner, Solid State Ionics **129**, 13 (2000).
[40] J. C. Ruiz-Morales, J. Canales-Vazquez, C. Savaniu, D. Marrero-Lopez, W. Z. Zhou, and J. T. S. Irvine, Nature (London) **439**, 568 (2006).
[41] X. Li, H. L. Zhao, F. Gao, N. Chen, and N. S. Xu, Electrochem. Commun. **10**, 1567 (2008).
[42] X. Li, H. L. Zhao, N. S. Xu, X. Zhou, C. J. Zhany, and N. Chen, Int. J. Hydrogen Energy **34**, 6407 (2009).
[43] X. Guoliang, X. Dong, K. Huang, and F. Chen, Mater. Res. Bull. **46**, 57 (2011).
[44] D. Neagu and J. T. S. Irvine, Chem. Mater. **23**, 1607 (2011).
[45] F. W. Lytle, J. Appl. Phys. **35**, 2212 (1964).
[46] G. Kresse and J. Furthmuller, Phys. Rev. B **54**, 11169 (1996).
[47] G. Kresse and D. Joubert, Phys. Rev. B **59**, 1758 (1999).
[48] J. P. Perdew, K. Burke, and M. Ernzerhof, Phys. Rev. Lett. **77**, 3865 (1996).
[49] H. J. Monkhorst and J. D. Pack, Phys. Rev. B **13**, 5188 (1976).
[50] Y. A. Abramov, V. G. Tsirelson, V. E. Zavodnik, S. A. Ivanov, and I. D. Brown, Acta Crystallogr. B **51**, 942 (1995).
[51] K. van Benthem, C. Elsasser, and R. H. French, J. Appl. Phys. **90**, 6156 (2001).
[52] J. Robertson, K. Xiong, and S. J. Clark, Thin Solid Films **496**, 1 (2006).
[53] C. Zhang, C. L. Wang, J. C. Li, K. Yang, Y. F. Zhang, and Q. Z. Wu, Mater. Chem. Phys. **107**, 215 (2008).
[54] See Supplemental Material at http://link.aps.org/supplemental/10.1103/PhysRevB.84.205102 for most dominant structures of doped $SrTiO_3$ identified in constrained *ab initio* thermodynamic calculations, summary of all reaction energies used in *ab initio* thermodynamic simulations, density of states of $SrTi_{0.6}Nb_{0.2}Ga_{0.2}O_{2.8}$, and calculated electronic band structure of selected materials.
[55] S. C. Ammal and A. Heyden, J. Chem. Phys. **133**, 164703 (2010).
[56] J. K. Norskov, J. Rossmeisl, A. Logadottir, L. Lindqvist, J. R. Kitchin, T. Bligaard, and H. Jonsson, J. Phys. Chem. B **108**, 17886 (2004).
[57] P. W. Atkins, *Physical Chemistry* (Oxford University Press, Oxford, 1998), pp. 485, 925–927, 942.
[58] S. Laursen and S. Linic, Phys. Chem. Chem. Phys. **11**, 11006 (2009).
[59] S. Laursen and S. Linic, J. Phys. Chem. C **113**, 6689 (2009).
[60] J. Rogal, K. Reuter, and M. Scheffler, Phys. Rev. B **75**, 205433 (2007).
[61] C. K. Gupta and A. K. Suri, *Extractive Metallurgy of Niobium* (CRC Press, Boca Raton, 1994).
[62] K. Kuroda, W. Sugimoto, M. Shirata, M. Takemoto, S. Hayami, and Y. Sugahara, Solid State Ionics **108**, 315 (1998).
[63] J. N. Yun, Z. Y. Zhang, J. F. Yan, and W. Zhao, J. Appl. Phys. **107**, 103711 (2010).